33RD CONGRESS
OF THE INTERNATIONAL COUNCIL
OF THE AERONAUTICAL SCIENCES
STOCKHOLM, SWEDEN, 4-9 SEPTEMBER, 2022

ICAS 2022 SWEDEN

COMBINED APPLICATION OF HYBRID LAMINAR FLOW CONTROL AND VARIABLE CAMBER IN PRELIMINARY AIRCRAFT DESIGN

Tim Effing[1], Victoria Schmitz[1], Florian Schültke[1], Fabian Peter[2] & Eike Stumpf[1]

[1]Institute of Aerospace Systems, RWTH Aachen University, 52062 Aachen, Germany
[2]Bauhaus Luftfahrt e.V., Willy-Messerschmitt-Str. 1, 82024 Taufkirchen, Germany

Abstract

In the design of conventional passenger aircraft, a major focus is on fuel efficiency and the associated reduction of emissions. Two promising technologies to increase aerodynamic efficiency and thereby reduce required tripfuel are hybrid laminar flow control and variable camber. Past research indicates favorable effects when combining these two concepts; however, the influence on overall aircraft level is still unknown. In this work, a method is derived enabling the investigation of the co-acting technologies in a preliminary aircraft design suite. This method utilizes a database holding aerodynamic data, which provides increased fidelity to map complex flow phenomena such as the laminar-turbulent transition. Preliminary studies on airfoil level are conducted allowing not only initial assessments of possible synergies between the technologies but also the formulation of guidelines for the subsequent database setup. The combined application of the two concepts is then evaluated on overall aircraft design level. For this, a stepwise approach is chosen, starting with a turbulent CS-25 technology demonstrator. Step-by-step, the single technologies are integrated and subsequently evaluated before the combination is finally analyzed. The results indicate considerable potential of the combined application with almost 5 % reduction in tripfuel for a medium range mission. However, further investigations should reveal even higher potential if the planform of the wing is optimized and additional variable camber flaps are integrated into the aircraft.

Keywords: Hybrid laminar flow control, Variable camber, Preliminary aircraft design, MICADO

1 Introduction

In 2019, the civil aviation industry was responsible for roughly 2 % of man-made carbon emissions. To contribute to climate change and minimize the expected impact on the industry, the International Air Transport Association (IATA) has set the goal to reduce net CO_2 emissions to 50 % of 2005 levels by 2050. [1] Further ambitious targets, such as reducing NO_x emissions by 90 % by 2050, are formulated in the European Commission's Flightpath 2050 [2]. The ongoing COVID-19 pandemic additionally poses acute new challenges to the aviation industry. Due to the declining passenger numbers and the reduced number of flights, not only operators have been severely affected by the crisis. Aircraft manufacturers, their suppliers, and other involved companies are also facing the challenges of the pandemic. One key factor for the aviation industry to not only overcome the crisis but also meet its climate goals by 2050 is the improvement of the aircraft's efficiency and the associated reduction in both costs and emissions.

For this, improving the aerodynamics of the aircraft offers great savings potential. Past research in aerodynamic technologies already led to continuous progress in the (conceptual) design of aircraft with reduced drag [3]; two promising technologies are hybrid laminar flow control (HLFC) and variable camber (VC). While the potential of the individual technologies has already been demonstrated in various publications [4, 5, 6, 7, 8, 9], their influence on the overall aircraft design (OAD) when simultaneously integrated is still an open research topic. To close this gap, the German LuFo VI-1

project *CATeW* (Coupled Aerodynamic Technologies for Aircraft Wings) was initiated; in this project, the influence of a combined application of HLFC and VC on a medium haul reference aircraft is investigated. The general idea is to maximize the effect of the technology composition in synergistic action; more precisely, VC permits to control the pressure distribution in cruise flight [10], which in turn can boost the laminar potential of HLFC. Further benefits and/or penalties may be revealed during the project. The work at hand presents an approach to design an aircraft with co-acting HLFC and VC technologies using the aircraft design environment MICADO[1]. After a short overview of the required fundamentals in Sec. 2, the work is divided into three parts:

1. Aerodynamic analysis of the combined application of HLFC and VC on airfoil level (Sec. 3);
2. Presentation of the methodology based on guidelines derived from pre-studies (Sec. 4);
3. Step-by-step retrofit design of aircraft with co-acting HLFC and VC technologies (Sec. 5).

2 Fundamentals

Improving the aerodynamic performance of an aircraft results in a reduction of its fuel consumption and in an increase in its overall efficiency. To evaluate the aerodynamic performance, the lift-to-drag ratio (L/D) is used [10]. One of the main drag components of an aircraft is the friction drag, which is primarily caused by the wing and adds up to more than 50 % of the overall cruise drag [14]. One viable way to reduce the friction drag is to delay the transition from laminar to turbulent flow. The transition is mainly triggered by the following three critical flow mechanisms: Tollmien-Schlichting instabilities (TSI), cross-flow instabilities (CFI), and Attachment-line transition (ALT). Whereas TSI are amplified by positive pressure gradients, CFI are amplified by negative pressure gradients; thus, TSI usually occur behind the maximum thickness of an airfoil, and CFI, in turn, occur at the leading edge of the wing [15]. ALT can lead to a fully turbulent flow over the wing due to the so-called leading edge contamination caused by turbulent disturbances [16]. One viable technique to address all three of those mechanisms is HLFC combining favourably shaped airfoils in the mid-region (natural laminar flow, NLF) and active suction of the boundary layer ahead of the front spar (laminar flow control, LFC). Utilizing a simplified suction concept [17], the potential of HLFC has recently been demonstrated in flight tests [18].

Although the wing of an aircraft is usually optimized for one design flight condition, in OAD, off-design conditions must be considered. During steady cruise flight, aircraft mass and thus lift coefficients change constantly, and continuous climbing would allow the aircraft to stay in its design optimum. Since such a mission profile is not compatible with current air traffic management, a compromise must be found [19]. To adapt to different flight conditions, the concept of the morphing aircraft proposes changing the geometry of the wing in-flight. The VC concept enables influencing the aerodynamic properties and optimizing the pressure distribution over the airfoil for each part of the cruise mission [20].

Since the off-design conditions may also result in a loss of laminar flow as the wing pressure distributions deviate from the optimum, the additional application of VC permits the pressure distributions to be kept in their design point [10, 21]. Due to strict requirements on the quality of the wing surface when integrating HLFC, Krueger flaps are used at the leading edge [22, 23]. This implies that VC systems can only be integrated at the trailing edge. Current examples for such VC concepts are the Variable Camber Continuous Trailing Edge Flap (VCCTEF), developed by NASA [24], and the Adaptive Dropped Hinge Flap (ADHF), which is already integrated in the Airbus A350 [25]. Both concepts utilize existing high-lift devices at the trailing edge of the wing. For VCCTEF, the flap is split into several segments that can be deflected individually, resulting in a higher effectiveness than conventional flaps [26]. The less complex ADHF concept utilizes the circular arc movement of a common dropped hinge flap to alter the wing area in-flight; the resulting gap is closed by an additional droop of the spoiler [27].

[1] Multidisciplinary Integrated Conceptual Aircraft Design and Optimization environment [11, 12]; MICADO is an internal specialization of UNICADO [13] providing methods with higher fidelity.

3 Preliminary studies on airfoil level

As stated in Sec. 1, past research already illustrated promising aerodynamic potential for both HLFC and VC, when applied individually. In this section, preliminary studies are conducted regarding the influence of airfoil deformations on the instability mechanisms relevant to transition; this is done to investigate whether an additional application of VC boosts the positive effects of the HLFC technology. The findings are then used to derive guidelines for the setup of an aerodynamic database, which is explained in detail in Sec. 4.3.

For the analyses in this section, a 2.5D toolchain developed by Risse [28] is used; this approach enables the consideration not only of TSI but also of CFI on airfoil level in an acceptable computing time. This is achieved by an iterative coupling of the 2D flow solver MSES [29] and the 3D transition prediction module STABTOOL [30, 31] using various transformation rules for both freestream conditions and geometry. Although ALT is not further addressed in this work, it is quantitatively evaluated in STABTOOL using the so-called Pfenninger-Poll criterion [32]. Since the focus is on the effects of different flap deflections on the transition point, an analysis of pure camber effects will be omitted. The objective is rather to investigate the effects of the combined technologies with different airfoil geometries and input flow conditions. This is achieved by using two different wing geometries and the associated differences in transformation angles; the two planforms are illustrated in Fig. 1.

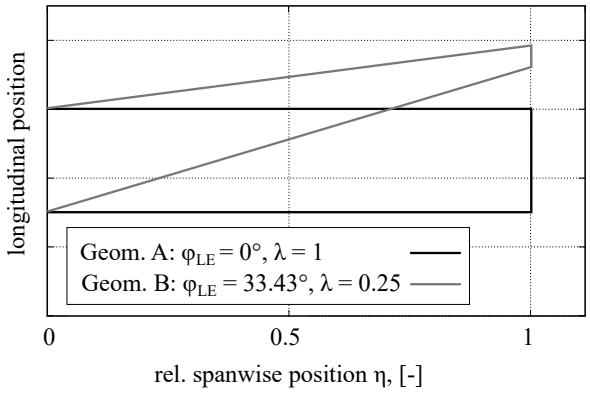

Figure 1 – Wing geometries used for pre-studies

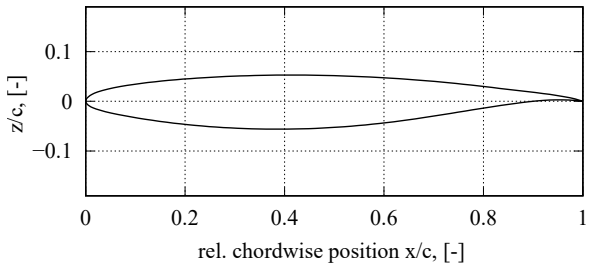

Figure 2 – Airfoil geometry used for pre-studies

Whereas for the unswept wing (*Geometry A*) only the two-dimensional TSI occur, both TSI and CFI must be considered for the swept wing (*Geometry B*). The calculations are conducted for various combinations of lift coefficient ($\mathrm{C_l}$) and Mach number (Ma). For the lift coefficient $\mathrm{C_l}$, values in the range of $0 \leq \mathrm{C_l} \leq 0.9$ with a step width of $\Delta\mathrm{C_l} = 0.05$ are considered for both geometries. The Mach numbers investigated are $0.5 \leq \mathrm{Ma} \leq 0.75$ for *Geometry A* and $0.7 \leq \mathrm{Ma} \leq 0.9$ for *Geometry B* ($\Delta\mathrm{Ma} = 0.05$). These ranges vary, since higher Mach numbers are not common for unswept wings. The ambient conditions of the freestream are set to those in 35000 ft using the ISA model.

The reference airfoil illustrated in Fig. 2 is used for all calculations within the pre-studies. This exemplary airfoil is chosen since it is part of the reference aircraft analyzed in Sec. 5. In Sec. 2, it was already discussed that the VC system can only be integrated at the trailing edge of the wing with VCCTEF and ADHF being promising concepts. Although both show significant advantages, the ADHF concept has—in the scope of the *CATeW* project—a higher weighted sum model score and has therefore been chosen for the further course of the project [33]. In order to simulate the different ADHF settings, the calculations within the pre-studies have to be carried out for various versions of the reference airfoil with different flap deflections. Therefore, seven different airfoil geometries are generated with flap angles $-2^\circ \leq \delta \leq 4^\circ$ ($\Delta\delta = 1^\circ$). In Fig. 3, the relevant components and hinge points are shown for the clean wing; additionally, two deployed airfoils are illustrated.

For all pre-studies, a constant suction distribution with two suction intervals is applied. The first linear interval ranges from the stagnation point to 8 % of the chord, and the second constant interval ranges from 8 % to 15 % of the chord. However, the reader should keep in mind that HLFC is only considered

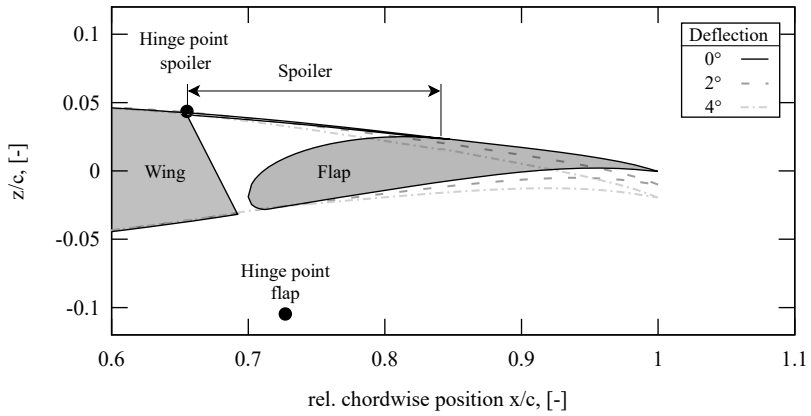

Figure 3 – ADHF airfoil rear sections for three different deployment angles

as a retrofit concept; the shape of the reference airfoil is not specifically optimized. Hence, only the application of suction up to the front spar combined with different flap deflections to simulate VC is considered.

In the following, a selected example from the preliminary studies of *Geometry A* is first presented, followed by a brief overview of the results of another example from *Geometry B*. These two cases provide a good overview of the occurring aerodynamic effects and can therefore be used representatively to derive guidelines for the creation of an aerodynamic database that can be queried from the aerodynamic module of MICADO (cf. Sec. 4.3).

To analyze the effect of the different flap settings with activated suction for *Geometry A*, the pressure distributions for exemplary freestream conditions of $\mathrm{Ma} = 0.75$ and $\mathrm{C_l} = 0.6$ are illustrated in Fig. 4a.

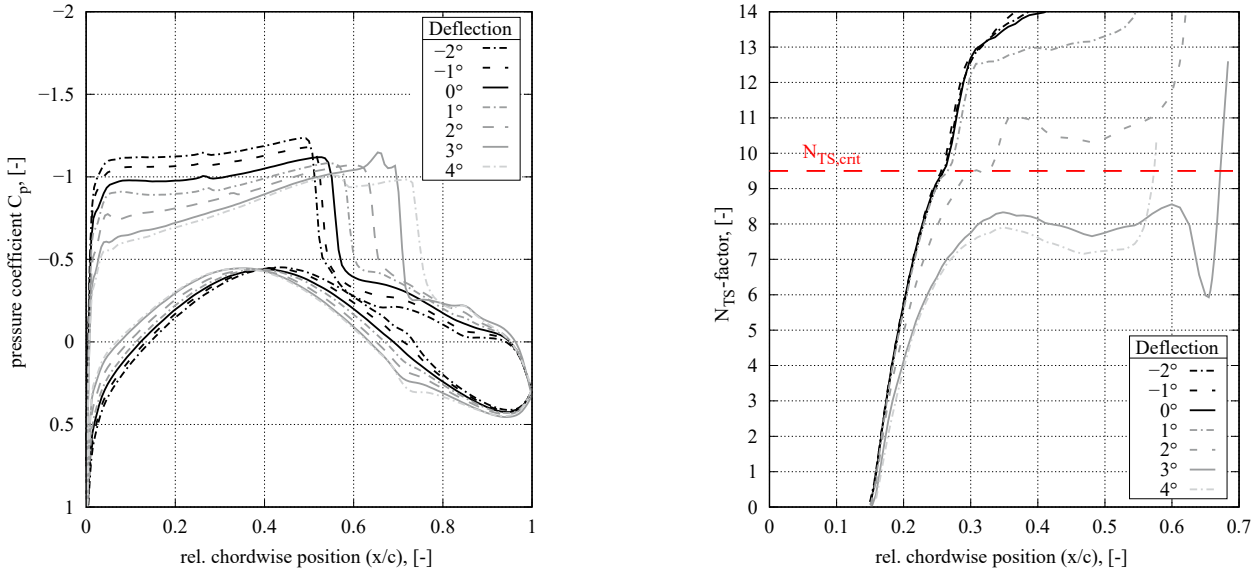

(a) Pressure distributions

(b) $\mathrm{N_{TS}}$ amplification

Figure 4 – Results for different flap settings of *Geometry A* at $\mathrm{Ma} = 0.75$ and $\mathrm{C_l} = 0.6$

It is evident that for the flap deflections in the range of $-2^\circ \leq \delta \leq 1^\circ$, the plateaus of the pressure distributions are nearly parallel to each other. In contrast, for deflections of $\delta \geq 2^\circ$, a greater negative pressure gradient can be observed, which has a stabilizing effect on TSI. Furthermore, the position of the shock moves downstream with increasing flap deflection; this enhances the extent of the flow with negative pressure gradients. Due to the spoiler droop, a local pressure peak can occur as it appears for the flap setting with $\delta = 3^\circ$. Since the wing considered in this case is unswept, neither CFI nor ALT

occur. To further analyze the behaviour of TSI, the amplification of the so-called N-factors[2] is used. The TSI envelopes corresponding to the pressure distributions presented in Fig. 4a are illustrated in Fig. 4b; the horizontal dashed line marks the critical $\mathrm{N_{TS}}$-factor of 9.5 [34] at which the transition from laminar to turbulent flow is assumed.

It can be seen that the amplification of TSI decreases with increasing flap deflections for $-2^\circ \leq \delta \leq 3^\circ$; this indicates a downstream shift of the transition for these deflection angles. For a flap deflection of $\delta = 4^\circ$, however, the transition point moves slightly upstream again, since a second shock is developing, whose positive pressure gradient decisively amplifies the TS waves (cf. Fig. 4a). Thus, a higher flap deflection does not necessarily lead to a greater delay of the transition.

Next, the effect of a flap deflection on individual drag components is analyzed exemplary for $\delta = 3^\circ$. In MSES, the following breakdowns of the profile drag ($\mathrm{C_{d,prof}}$) are available:

$$C_{d,prof} = \overbrace{C_{d,fric} + \underbrace{C_{d,visc-p}}_{C_{d,pres}}}^{C_{d,visc}} + C_{d,wav} \tag{1}$$

For all aerodynamic calculations in MICADO, the breakdown in viscous ($\mathrm{C_{d,visc}}$) and wave drag ($\mathrm{C_{d,wav}}$) is usually used. The calculated drag values for exemplary flow conditions of $\mathrm{Ma} = 0.75$ and $\mathrm{C_l} = 0.6$ are summarized in table 1.

Table 1 – Drag coefficients at $\mathrm{Ma} = 0.75$ and $\mathrm{C_l} = 0.6$

Parameter	**Unit**	**Deflection**		**Δ, [%]**
		0°	3°	
$\mathrm{C_{d,visc}}$	dc	62.7	51.6	-17.7
$\mathrm{C_{d,wav}}$	dc	29.1	20.5	-29.6
$\mathrm{C_{d,prof}}$	dc	91.8	72.1	-21.5

The deflection of the flap and the associated delay of the transition from laminar to turbulent flow reduces the viscous drag by 11.1 dc[3]. Since the shock strengths do not differ significantly (cf. Fig. 4a), the changes in wave drag are attributed to the respective angle of attacks (AoAs) and the corresponding flow separation; the AoAs differ if a constant $\mathrm{C_l}$ is set by the user. The wave drag changes as the square of AoA [35], and a smaller AoA is required with increasing flap deflection ($\mathrm{AoA}_{\delta=0^\circ} = 1.35^\circ$ vs. $\mathrm{AoA}_{\delta=3^\circ} = -0.87^\circ$). Thus, the wave drag is also reduced. Compared to the clean airfoil, the flap deployment leads to an overall profile drag reduction of 21.5 %. The extent to which this observation covers the entire $\mathrm{C_l}$ range is analyzed using Fig. 5, which illustrates the associated drag polars for $\mathrm{Ma} = 0.75$ and the two flap settings.

For lift coefficients $\mathrm{C_l} \leq 0.55$, the deflected airfoil has a slightly increased wave drag. This is mainly due to minor shock developments already for lower lift coefficients. At all other values, the drag is significantly reduced as both the shock strength and the required angle of attack change. Due to a downstream shift of the transition point, the viscous drag is reduced for $\mathrm{C_l} \leq 0.65$ for the deployed airfoil; for higher $\mathrm{C_l}$, this potential is neglected, since TS waves are increasingly amplified and shift the transition upstream. In total, however, the combined application of HLFC and VC increases the efficiency of the airfoil in the presented case. Nonetheless, a reduction of the profile drag does not necessarily occur for all flow conditions and increasing flap deflections; this is illustrated with another example using an airfoil cut at $\eta = 0.5$ of *Geometry B* for $\mathrm{Ma} = 0.85$. In this case, both TSI and CFI influence the transition position and are therefore considered in STABTOOL. In Fig. 6, the transition characteristics, i.e. maximum N-factors and transition point, are illustrated as a function of lift coefficient for $\delta = 0^\circ$ and $\delta = 3^\circ$.

[2]The N-factors result from a linear stability analysis within the STABTOOL submodule LILO [31].

[3]One drag count (dc) equals $\mathrm{C_d} \cdot 10^4$.

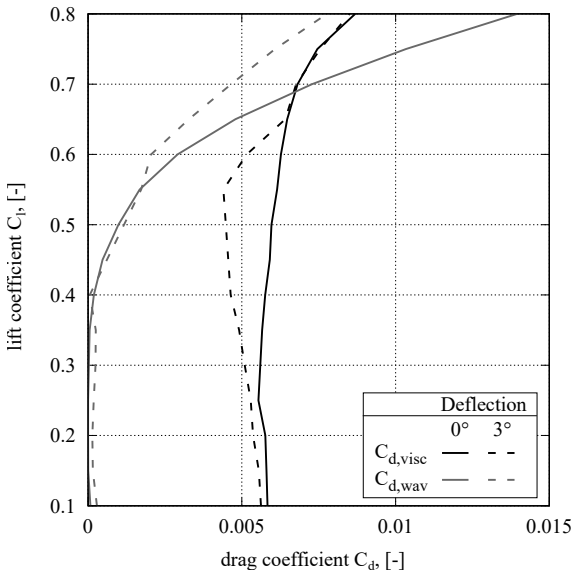

Figure 5 – Drag polars of *Geometry A* at $\mathrm{Ma} = 0.75$

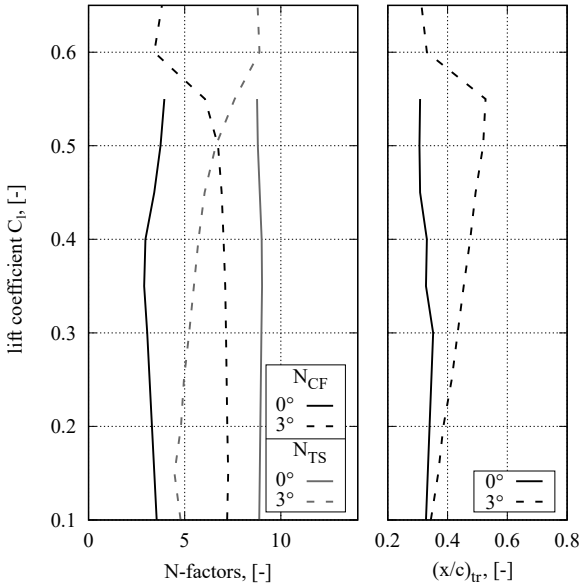

Figure 6 – Transition characteristics of *Geometry B* at $\mathrm{Ma} = 0.85$

The left side of Fig. 6 reveals that the deployed ADHF flap—compared to the clean airfoil—increases the amplification of cross-flows but simultaneously damps the Tollmien-Schlichting waves. Although the critical N_{CF}-factor of 7.5 [34] is reached for almost the entire C_l range, the data on the right side of Fig. 6 shows no transition at the leading edge. Thus, $N_{CF,crit}$ is only reached due to a re-amplification of cross-flows downstream, which does not trigger the CF typical transition directly at the leading edge. The transition is therefore rather initiated if a pair of N_{TS}- and N_{CF}-factors intersects the critical curve obtained from both critical factors. This pair, however, is positively influenced by the flap deployment resulting in a shift of the transition position for almost every lift coefficient. Interestingly, despite the delayed transition, the polars of the deployed airfoil in Fig. 7a show increased drag for both viscous and wave drag coefficients.

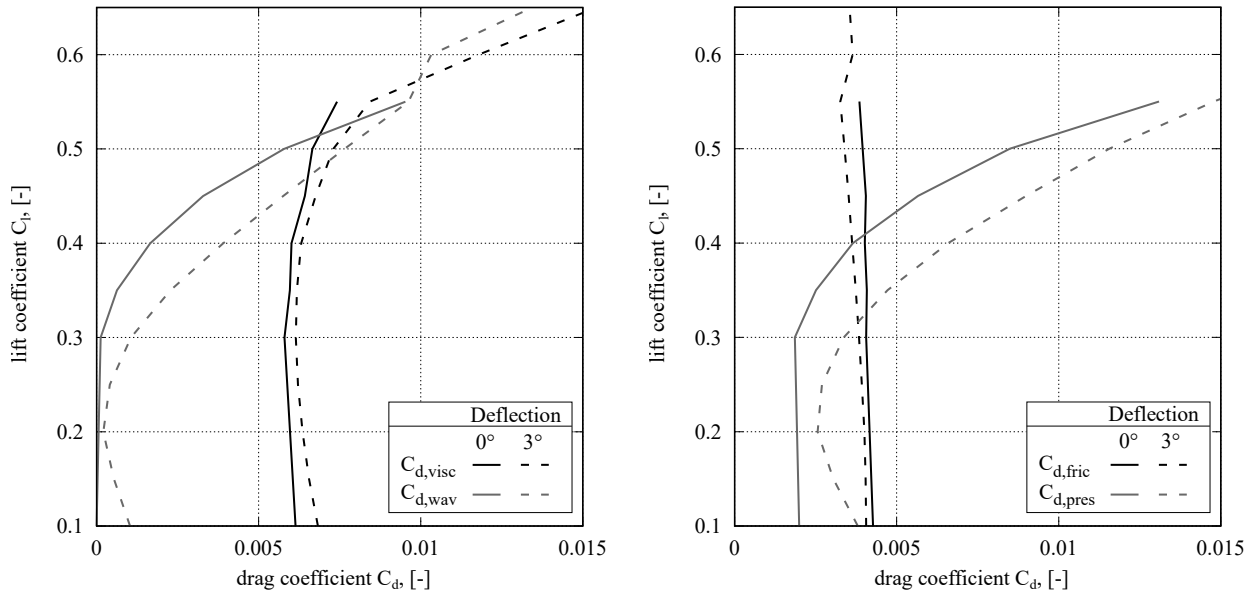

(a) Viscous and wave drag polars

(b) Friction and pressure drag polars

Figure 7 – Drag polars of *Geometry B* at $\mathrm{Ma} = 0.85$

To further analyze this effect, the alternative drag breakdown from Eq. 1 is used; the respective polars are shown in Fig. 7b. It can be seen that the friction drag follows the transition shift in Fig. 6,

leading to a delta in the respective polar, which increases with $\mathrm{C_l}$. Hence, the decisive factor for the increased profile drag is the pressure drag, which is mainly determined by the differences in shock strengths and angle of attack values. All in all, for *Geometry B*, the deflection of the ADHF leads to an increase in the overall profile drag over the entire range of considered lift coefficients for $\mathrm{Ma} = 0.85$.

Based on the observations described above and the results from the calculations that are not presented in detail in this paper, the following conclusions are derived for the creation of an aerodynamic database:

- The combined application of HLFC and VC can be reasonable with regard to an overall drag reduction.
- For the combinations of Ma and $\mathrm{C_l}$ considered above, negative flap deflections do not contribute to the delay of the transition of the flow.
- Positive flap deflections can contribute to the delay of the flow transition; however, the larger the flap angle, the more detrimental effects such as increased pressure drag must be considered. This indicates the existence of an upper boundary for the airfoil deflections for the database setup.
- For positive flap deflections, a significant reduction in profile drag was observed in the example considered in detail; this can be attributed in particular to the lower wave/pressure drag. Nonetheless, the second example illustrated that an increase in profile drag can occur despite a reduction in friction drag.

$\Rightarrow$ It must therefore be decided individually for each case whether an additional deflection of the VC system is useful, and which flap position should be selected to achieve the desired result. Thus, a database should cover all possible combinations of input parameters to allow maximum choice in the overall aircraft design.

4 Method for combined application of HLFC and VC

Prior research conducted at ILR enabled the evaluation of both HLFC and VC. In the past, however, the two methods for HLFC and VC were used independently. In this work, we present a combination of both approaches, which therefore efficiently uses synergies from the research conducted at ILR during the last years. In the following, the approach is described top-down: Starting from OAD level in Sec. 4.1, we then present the aerodynamic calculation in Sec. 4.2, before the handling and the setup of the underlying 2D airfoil database is described in Sec. 4.3.

4.1 Overall aircraft design

In MICADO, any aircraft without VC application, be it a turbulent reference or an HLFC retrofit, is usually designed utilizing the entire design loop illustrated in Fig. 8. For aircraft with integrated VC technology, however, only a simplified version of the MICADO toolchain is executed. Hence, the already converged reference aircraft is not re-designed but rather analyzed for a specific study mission using one VC polar (cf. Fig. 9). The idea of this approach, which was developed by F. Peter at ILR, is to design a reference aircraft without integrated VC technology, and assess the potential of deployed flaps on a separate mission. No particular VC system design needs to be considered, since not the flap loads from VC application but rather the high-lift performance determines the actuator sizing. The only mass components that are not considered are additional gear boxes; these, however, have a negligible influence on the final design. [36]

If the HLFC technology is additionally integrated, a specific HLFC system design is used to cover detrimental effects of the additional power offtakes during the study mission (dashed box in Fig. 9). This is mandatory since—in contrast to VC—HLFC adds new components, such as compressors and ducts, to the system architecture of the aircraft. For this system, the simplified suction concept developed in the European ALTTA project for an Airbus A320 fin is used [17]; the basis for the design

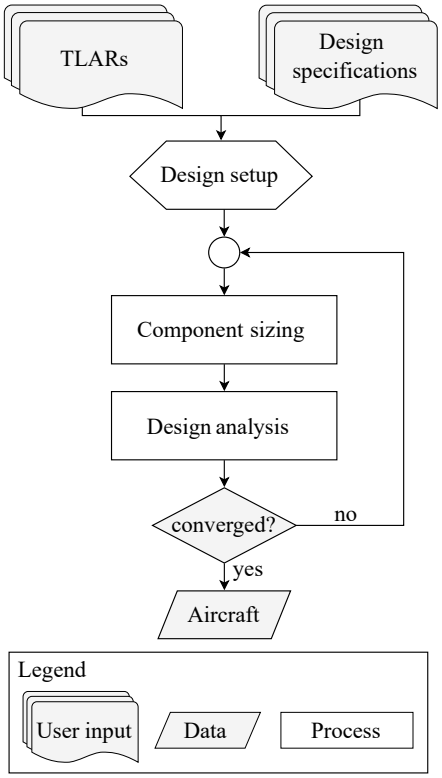

Figure 8 – MICADO toolchain

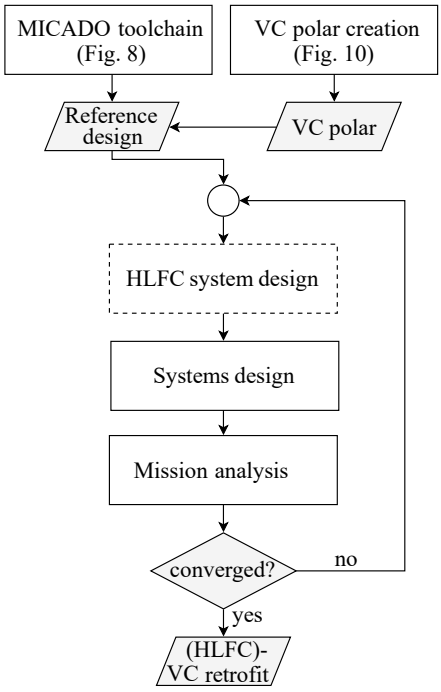

Figure 9 – Process for (HLFC)-VC retrofit

is a selection of methods and equations proposed by Pe and Thielecke [37]. Subsequent to the system analysis, the mission is simulated. For this, the cruise mission profile is optimized by maximizing the specific air range (SAR). This is done by automatically selecting the initial cruise altitude and constantly checking if a step climb would yield a better SAR. Convergence of this process using, e.g., the take-off mass as a criterion, results in the final (HLFC)-VC retrofit design.

4.2 Calculation of VC polar

The general idea of having only one VC polar is to calculate drag polars for every possible combination of airfoil permutations and to subsequently merge them according to a predefined criterion. In Fig. 10, the process chain to calculate a VC polar for the combined application of VC and HLFC is illustrated; the parts, which are exclusive for one of the technologies, are highlighted with blue boxes for HLFC and red boxes for VC, respectively.

The process starts by choosing geometric key points, i.e. the inner and outer stations of every segment, for a given wing geometry. After the creation of permutated VC airfoils (cf. Fig. 3) and the geometric transformation to 2D according to Risse [28], an aerodynamic database is set up with MSES using an approach developed by Schültke [38]. Since this airfoil database is a key element for all current research regarding HLFC and VC at ILR, the setup and handling is described separately in Sec. 4.3. Once the database is available, a set of wing permutations is derived, each representing a different combination of airfoil permutations along the wingspan. For every wing permutation, the aerodynamic module of MICADO is then used to calculate viscous and wave drag components from the database. To reduce computation time, the database approach is optionally executed only for specific Mach numbers, such as the cruise Mach number, at which both technologies are activated. The other polars are then determined using semi-empirical relations from Raymer [39] for viscous drag and from Korn-Mason [40, 41] for wave drag. Combined with the induced drag component calculated with DLR's multiple-lifting-line code LIFTING_LINE [42, 43], single aircraft polars are obtained from the aerodynamic module. The polars for every wing permutation are finally merged into one VC polar; this is done by identifying the wing permutation with the best lift-to-drag ratio for every polar point [44].

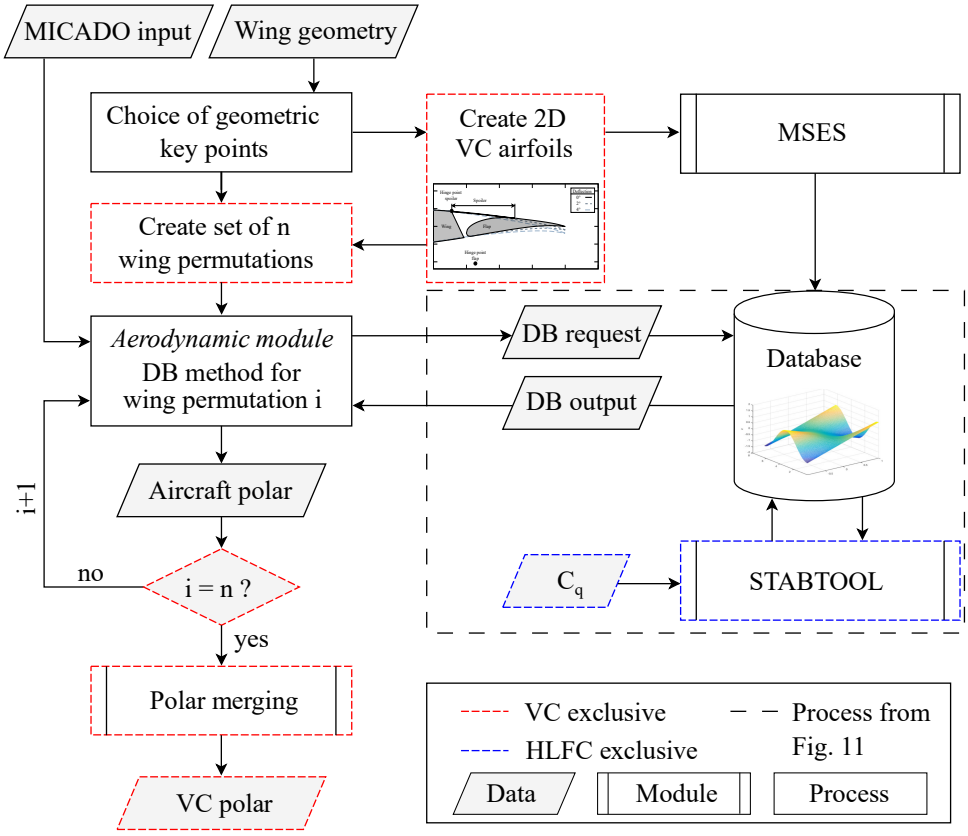

Figure 10 – Process chain to derive VC polar for HLFC and VC application

4.3 2D database approach

The pre-studies in Sec. 3 were conducted with the 2.5D method developed by Risse [28]. Combining the 2D flow solver MSES and the 3D stability analysis program suite STABTOOL on airfoil level allows rapid and consistent prediction of drag polars before storing the (laminar) data in an aerodynamic database and subsequently feeding it back into the overall design loop. In the course of the last years, however, results from internal and external projects of the ILR led to various changes in the toolchain for the aerodynamic drag prediction. These changes by Schültke [38] mainly concern the setup of the aerodynamic database and the data processing within the database. Contrary to the method proposed by Risse [28], the new approach foresees the setup of a database holding solely aerodynamic 2D data; this results in a de-coupling of MSES and STABTOOL. In addition, automatic data refinement and sophisticated interpolation methods ensure sufficient data quality for the subsequent design process. In Fig. 11, the new approach for querying the database is illustrated.

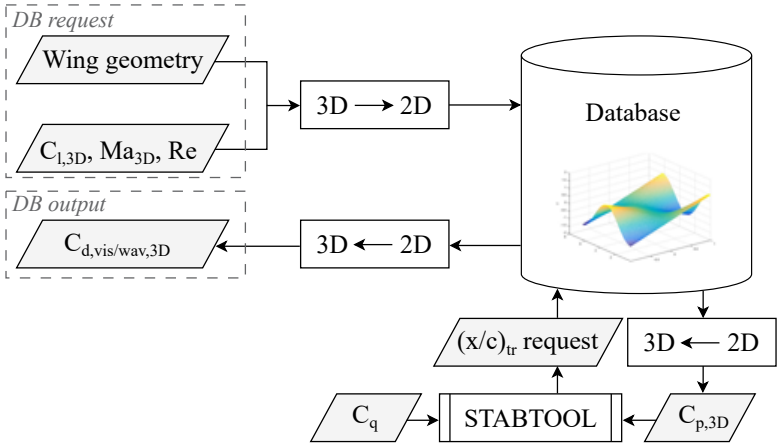

Figure 11 – New approach for aerodynamic drag prediction in MICADO

Compared to the prior approach, the input and output data of a database query remain unchanged. Thus, the database provides viscous and wave drag coefficient for known freestream conditions and the respective wing geometry. However, since it holds 2D data, STABTOOL is now executed during the aircraft design process. The essential advantages over the previous approach are:

- The database is independent of a specific wing geometry, since the transformation rules are only applied when the data is queried during the design loop. Thus, the airfoil-specific data needs to be only calculated once and can then be used for any further aerodynamic analyses.
- The influence of the Reynolds number (Re) on the prediction accuracy of the drag polars is addressed more accurately; i.e., abrupt shifts of the transition position, which were demonstrated in Ref. [45], can be sufficiently taken into account.
- Automatized post-processing steps allow the identification of characteristic parameters such as the drag-divergence Mach number for each lift coefficient; these parameters can be used, e.g., in a novel wing design method that is subject of current research at ILR.
- The integration of STABTOOL into the overall design loop permits variations of the suction distribution without the need to set up a new database.

This new approach is used for all airfoils of the given wing geometry to calculate aerodynamic data for numerous variations of lift coefficient, Mach number, and Reynolds number. The application of HLFC adds the transition position as another dimension [38]; this one is required to get data for the laminar-turbulent transition position, which is determined live during the aircraft design with MICADO using STABTOOL. In contrast, the VC technology comes in place by setting up a database not only for the clean airfoils but also for various permutations of eligible airfoils along the wingspan. For the combined application of the two technologies, the database is therefore set up for a predefined range of the five dimensions $\mathrm{C_l}$, Ma, Re, $(\mathrm{x/c})_{\mathrm{tr}}$, and the airfoil's deployment angle δ.

5 Application cases

In this section, we apply the developed methodology for integrating the combined application of HLFC and VC in MICADO to different use cases. The reference aircraft and the relevant design conditions are introduced first. Afterwards, the results of the step-by-step approach to derive an aircraft with integrated HLFC and VC technologies are presented.

5.1 Reference aircraft

For the reference aircraft, the turbulent CS-25 technology demonstrator CATeW-02 is used. This medium range aircraft for 252 PAX and a cruise Mach number of $\mathrm{Ma_{cr}} = 0.83$ originates from the German LuFo V-3 project *AVACON* [46], and was slightly adapted in the *CATeW* project due to findings discussed in Ref. [33]. In Fig. 12, the segmented wing planform, which comes with a reference area of 220 m^2 and a leading edge sweep of $\varphi_{\mathrm{LE}} = 33.43°$, is illustrated.

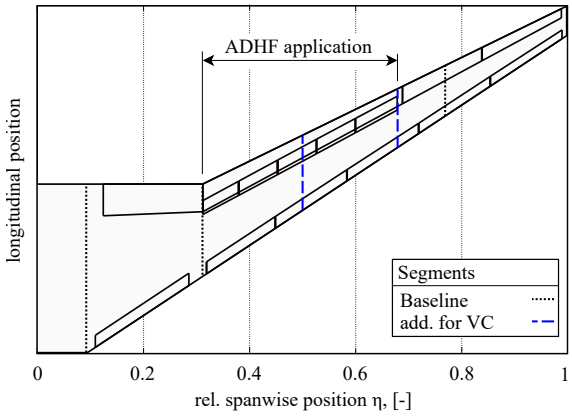

Figure 12 – Planform of the reference wing

It can be seen that two additional segments are added to prepare for the ADHF application in the later use cases. The application area is limited by the available spoilers of the reference aircraft. Hence, no inboard actuation is considered; to what extent this application area might need to be adapted will be discussed in Sec. 5.2.4. For all airfoil cuts highlighted in Fig. 12, the aerodynamic 2D database is set up as described in Sec. 4.3. If the airfoil is in the ADHF application area, deployment angles in the range of $-2° \leq \delta \leq 4°$ with steps of $\Delta\delta = 1°$ are additionally considered. With this database, the reference aircraft can be designed using the MICADO toolchain from Fig. 8. The resulting key design parameters of the converged turbulent aircraft are listed in table 2.

Table 2 – Key parameters of turb. baseline

Parameter	Unit	Value
Maximal take-off mass (max. TOM)	t	137.09
Operating empty mass (OEM)	t	79.62
$(L/D)_{opt}$	-	19.84
Tripfuel design mission ($TF_{4600\,NM}$)	t	28.67

5.2 Design of a retrofit aircraft with integrated HLFC and VC technologies

The retrofit aircraft with integrated HLFC and VC technologies is derived from the turbulent reference aircraft with the following step-by-step approach:

1. Retrofit design with integrated HLFC (Sec. 5.2.1);
2. Retrofit design with integrated VC (one and two VC flap configuration; Sec. 5.2.2);
3. Retrofit design with both HLFC and VC (one and two VC flap configuration; Sec. 5.2.3).

Hence, the individual technologies are first analyzed separately before the final design with combined application of HLFC and VC is derived; all results are then discussed in Sec. 5.2.4. This approach helps in the evaluation of the final design and in the analysis of whether or not the advantages of the individual technologies can be transferred to an overall benefit.

5.2.1 HLFC retrofit design

In order to investigate the influence of HLFC on aircraft performance, various steps must be taken beforehand to derive a retrofit design. For this purpose, the design guidelines presented by the author in Ref. [47] are used.

The laminar retrofit utilizes Krueger flaps as high-lift systems on the leading edge to passively prevent contamination (cf. Sec. 2); this results in the boundary layer suction being only possible on the upper side of the wing. In addition, the HLFC system design module is included in the MICADO toolchain. For all following studies with integrated HLFC technology, the HLFC system has three decentralized compressors per wing side and a so-called collective ducting architecture, in which the sucked air of all compressors is transported through a central duct to the outlet at the wing-fuselage junction. For the HLFC system, suction distributions are used that are comparable to the ones determined to be optimal for a similar aircraft in Ref. [47]; for the additional VC segments (cf. Fig. 12), these distributions are used as key points for interpolation. The suction distributions and the resulting HLFC system architecture are depicted in Figs. 13 and 14, respectively.

Similar to the suction distribution used for the pre-studies in Sec. 3, both distributions are composed of two linear intervals; the different end points are due to the changing relative front spar positions along the wingspan. The resulting HLFC system for the converged laminar retrofit aircraft comes with a total mass of approx. 256 kg and an electric power requirement of approx. 106 kW.

Starting with the aerodynamic analysis, the laminar area for the optimum lift coefficient in cruise flight is illustrated in Fig. 15.

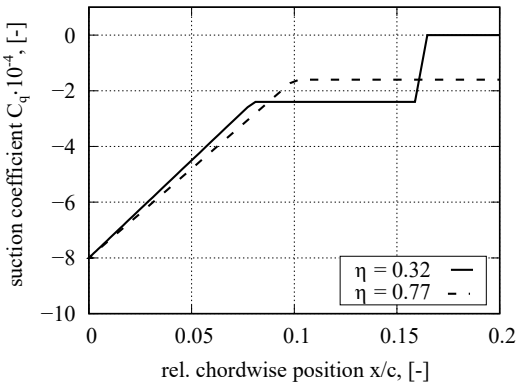

Figure 13 – Selected suction distributions

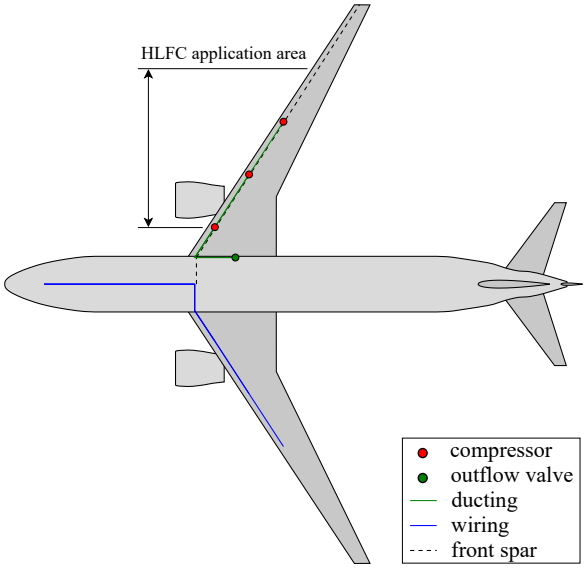

Figure 14 – HLFC system architecture

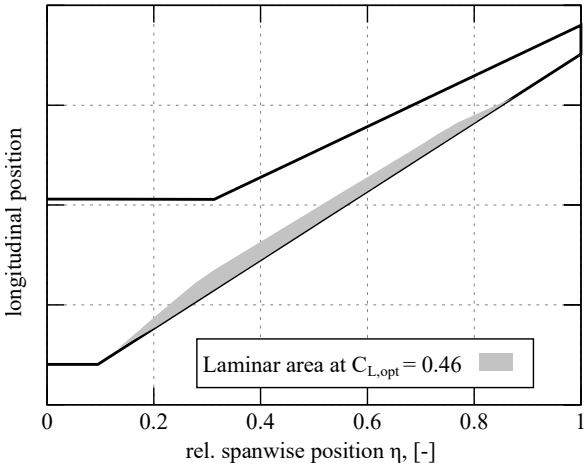

Figure 15 – Laminar area in cruise flight

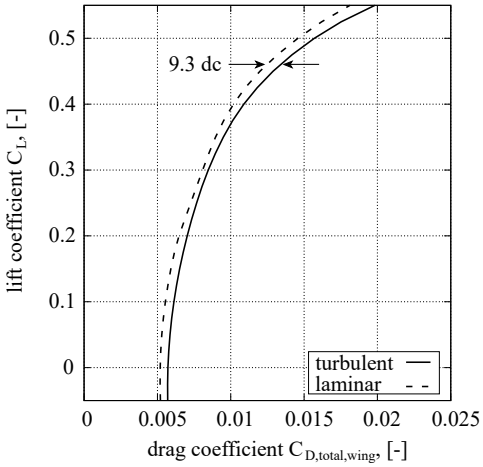

Figure 16 – Shift of wing polars

It is evident that cross-flow instabilities are sufficiently suppressed with the selected suction distribution. After a slow build up starting from the fuselage-wing junction, however, the laminar area in chordwise direction is limited roughly by the end of the local suction distribution. Hence, similar to the behavior shown in Fig. 4b, TSI waves are strongly amplified after the end of the suction. Since the suction distribution is limited by the front spar position, the only way to further increase the laminar area is to optimize or change the used airfoil geometries and/or the whole planform. Nonetheless, the laminar area leads to a shift of the wing polars, which is illustrated in Fig. 16.

As shown in Fig. 16, the integration of the HLFC system and the thereby achieved laminar area shift the wing polar to considerably lower drag coefficients. For the highlighted exemplary lift coefficient $C_L = 0.46$, a reduction of more than 9 dc is achieved. The HLFC retrofit design is finally derived by feeding the aerodynamic data back into the MICADO design loop, calculating mass components and system offtakes, and simulating the mission until convergence is achieved. The approach used within this work does not involve any geometric resizing and shape optimization. Therefore, the integration of HLFC is a pure 'add-on' to the turbulent design. However, not only aerodynamic benefits but also detrimental effects of integrating the HLFC system, such as additional masses and decreased engine performance due to additional power offtakes, are considered. In Fig. 17, the relative percentage change of the key parameters of the converged HLFC retrofit compared to the turbulent reference (TR) are shown.

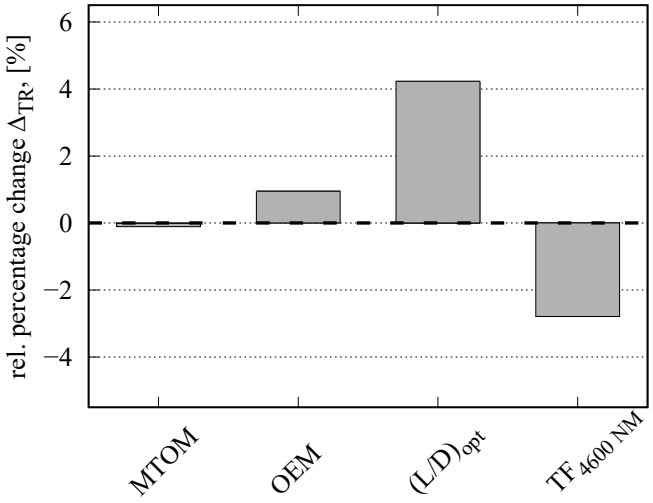

Figure 17 – Rel. percentage change of HLFC retrofit compared to turbulent reference

Although the integration of the additional HLFC system components and the resizing of the other components result in an almost 1 % increase in OEM, the TOM is slightly reduced. This is due to the improved aerodynamics and the corresponding reduction in tripfuel of almost 2.8 %; this limited savings potential is revisited and discussed in Sec. 5.2.4.

5.2.2 VC retrofit design

In this section, two different VC retrofit designs are presented; both designs are derived from the turbulent baseline introduced in Sec. 5.1. The first design uses the ADHF application area highlighted in Fig. 12 only with uniformly deployed flaps simulating one large ADHF flap. The second one splits the available area in two ADHF segments and thus allows different flap settings. Hence, the influence of different number of outboard ADHF flaps can be analyzed.

Starting again with the aerodynamics, the turbulent reference polar as well as the VC polars created with the process described in Sec. 4.2 are shown; for the best possible visualization, the $\mathrm{L/D}$ is plotted over $\mathrm{C_L}$ for the cruise Mach number.

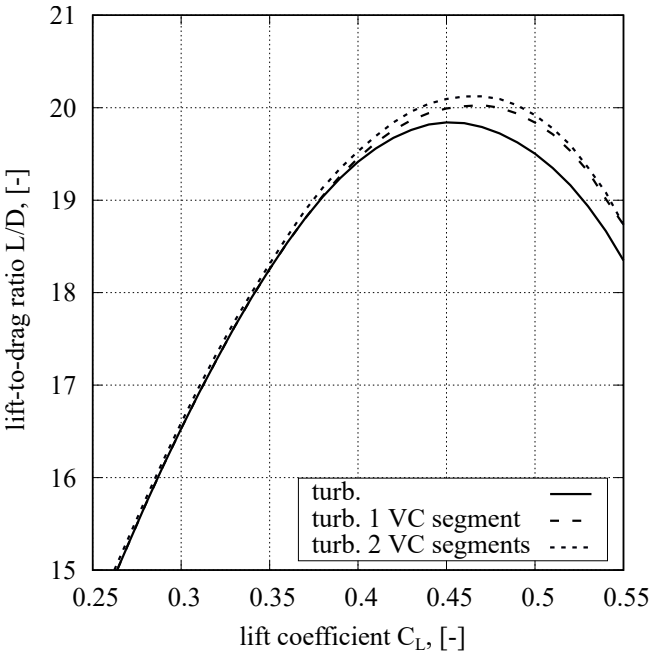

Figure 18 – Cruise $\mathrm{L/D}$ polars for turbulent aircraft with and without VC application

The polars show that the application VC results in higher aerodynamic efficiency; this holds especially for the lift coefficients relevant for steady cruise flight, i.e. $0.4 \leq \mathrm{C_L} \leq 0.55$. Compared to the aircraft with one VC flap, the additional flap settings possible with the split flap increase the performance only slightly. Using these VC polars according to Fig. 9, the VC retrofit aircraft can be designed and assessed for the design mission with a range of 4600 NM. The resulting mission profiles, the lift coefficient profiles with the typical sawtooth-like contour, and the corresponding flap settings are illustrated in Fig. 19.

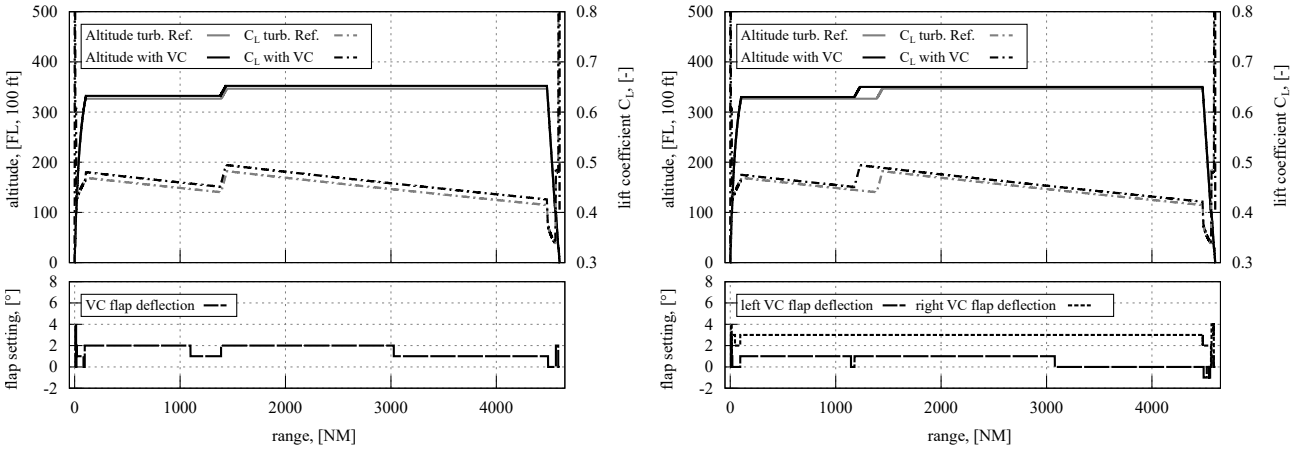

(a) Mission data with one VC flap

(b) Mission data with split VC flap

Figure 19 – Mission profiles and flap settings for turbulent VC application

Compared to the turbulent reference, there are no significant differences in the cruise profiles. The interval of the lift coefficients equals the optimum range of the $\mathrm{L/D}$ curve in Fig. 18; this results in slightly increased lift coefficients for both aircraft with integrated VC technology. The flap settings in the lower part of the figures indicate the use of the aerodynamic VC benefits from Fig. 18 over almost the whole mission. For the aircraft with one VC flap (Fig. 19a), the flap angle varies between $1^\circ \leq \delta \leq 2^\circ$. The drop before the step climb indicates that the decreasing lift coefficients lead to a point where the 1° flap setting is superior to the one with 2°. The step climb shifts the lift coefficients to higher values resulting in the 2° flap position being more favorable again. Figure 19b shows similar findings for the left flap. The right flap, however, is at 3° throughout the whole cruise; this indicates either an unsuitable design point of the associated airfoils or a suboptimal initial lift distribution for the present $\mathrm{C_L}$ range in cruise. In Fig. 20, the relative percentage changes compared to the turbulent reference are shown for both VC retrofits.

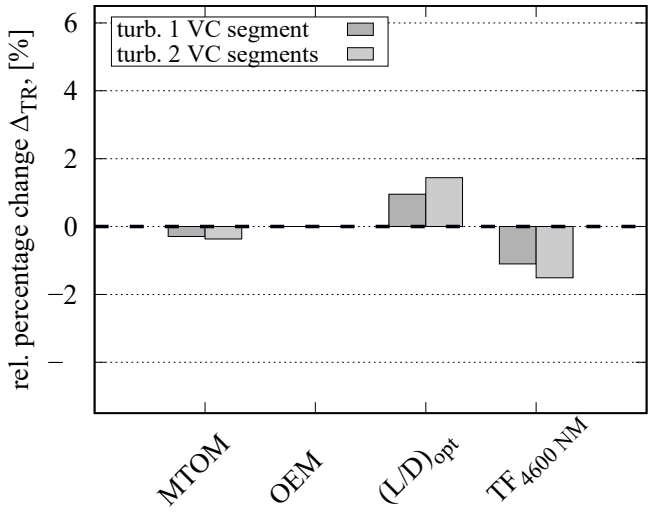

Figure 20 – Rel. percentage change of VC retrofits compared to turbulent reference

Since the additional gear boxes are neglected (cf. Sec. 4.1), no additional systems need to be added for the VC application; hence, the OEM does not change. Therefore, the reduction in TOM is even higher than for the HLFC retrofit, although both the aerodynamic benefit and the reduction in tripfuel are inferior to the results in Fig. 17. For the 4600 NM mission, the aircraft with one and two VC segments achieve a reduction in tripfuel of about 1.1 % and 1.5 %, respectively.

5.2.3 Combined application of HLFC and VC

Lastly, both technologies are integrated simultaneously using the full functionalities of the processes depicted in Figs. 9 - 11. For the underlying reference design, the HLFC retrofit from Sec. 5.2.1 is used. Therefore, all changes applied to the turbulent baseline are again considered. On top of that, laminar VC polars are calculated for configurations with one and two flaps. The resulting polars are presented in Fig. 21.

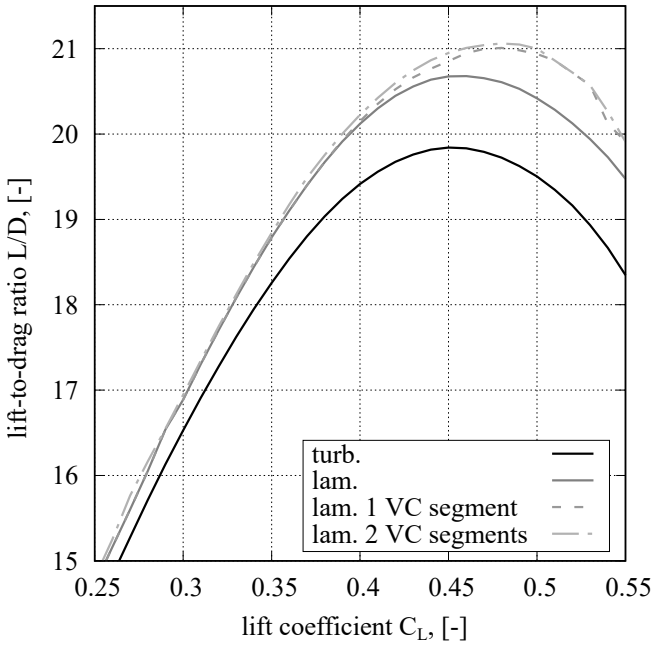

Figure 21 – Cruise L/D polars for laminar aircraft with and without VC application

Compared to the turbulent polar, the already shifted laminar polar is further improved due to the application of VC. As already seen in Fig. 18, the split flap only marginally increases the maximum aerodynamic performance. The optima of the lift coefficients, however, are shifted to higher values; this is also evident in the lift coefficient contours shown in Fig. 22.

The mission profiles of both configurations show that the automatically chosen initial cruise altitude is roughly 100 ft (or 10 FL) higher than for the turbulent reference. Therefore, the better SAR in higher altitudes due to the improved aerodynamics overbalances the additional fuel required for the longer climb segment. As already analyzed for the turbulent VC retrofits, different flap positions are chosen throughout the mission, with the right flap in Fig. 22b being the only one with a constant deployment angle of 3°. Figure 23 shows the relative percentage change of the different key parameters, again compared to the turbulent reference.

Since no resizing of the mass components is done, the increased OEM is transferred from the HLFC retrofit (cf. Fig. 17). However, the additional application of VC and the subsequently improved aerodynamics lead to a reduction of the tripfuel of 4.5 % for the one flap configuration and 4.8 % for the two flap configuration.

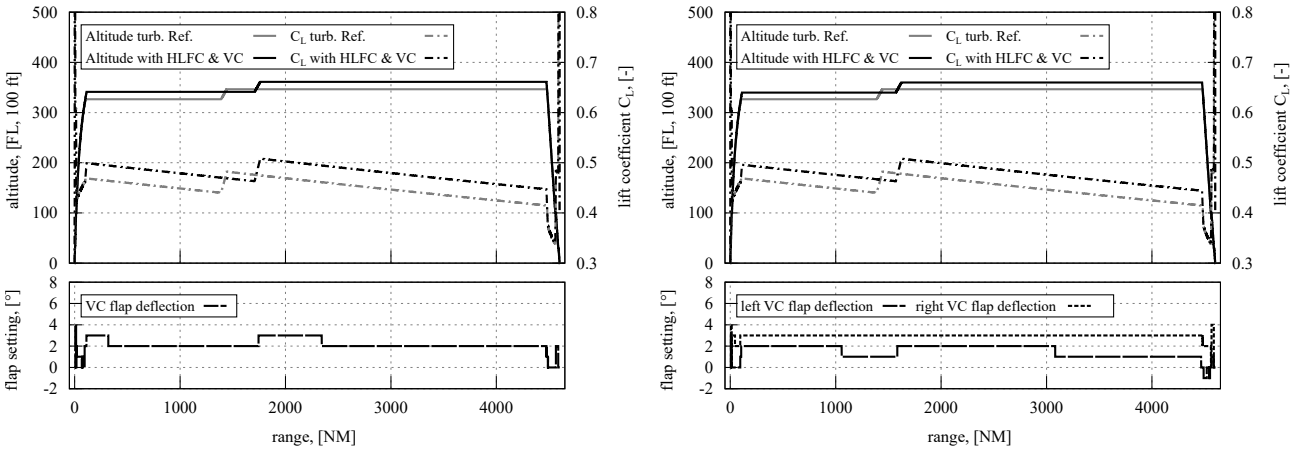

(a) Mission data with HLFC and one VC flap

(b) Mission data with HLFC and split VC flap

Figure 22 – Mission profiles and flap settings for HLFC and VC application

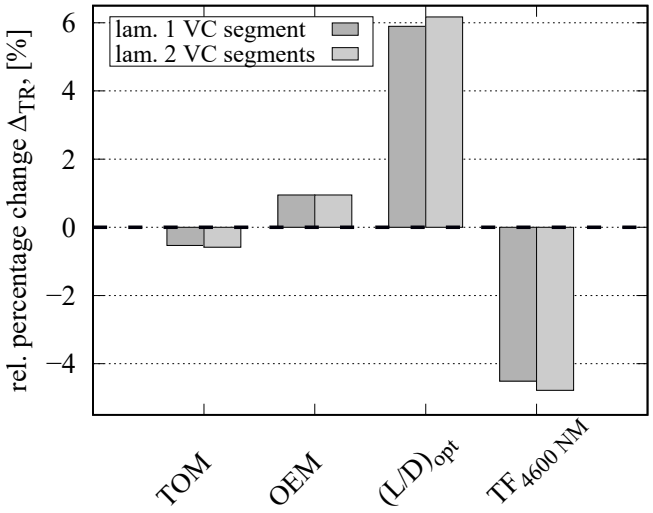

Figure 23 – Rel. percentage change of retrofits with HLFC and VC compared to turbulent reference

5.2.4 Result discussion

In this section, the results from the prior sections are summarized and classified using other research conducted at ILR. In table 3, a summary of the relevant key parameters is given for all configurations discussed.

Table 3 – Summary of key parameters of all discussed aircraft

Configuration	VC segments	MTOM, [t]	OEM, [t]	$(L/D)_{opt}$, [-]	TF, [t]	ΔTF_{TR}, [%]
turb. Ref.	0	137.09	79.62	19.84	28.67	-
HLFC retrofit	0	136.94	80.37	20.68	27.87	-2.8 %
VC retrofit	1	136.74	79.62	20.03	28.36	-1.1 %
	2	136.59	79.62	20.13	28.24	-1.5 %
HLFC & VC retrofit	1	136.36	80.37	21.01	27.38	-4.5 %
	2	136.29	80.37	21.06	27.30	-4.8 %

It is evident that the individual application of both technologies improve the overall design with the HLFC technology offering more tripfuel reduction than VC. Compared to the retrofit design presented in Ref. [48], however, the HLFC retrofit offers less than half the potential savings. To put this into perspective, it is noted that—although the general design settings and geometric properties are the same—a few differences occur between the design presented in this work and the one from Ref. [48]:

The used suction distributions were not specifically optimized for this reference aircraft and differ in both spanwise and chordwise suction lengths. On top of that, different 2D airfoil geometries are used, which seem to have less NLF potential and are therefore not suited to delay the transition much further after the front spar. This is in good agreement with findings in Ref. [33], where a laminar area similar to the one in Fig. 15 was predicted for the same outboard wing using high-fidelity computational fluid dynamics methods. Nonetheless, increasing this potential will be revisited in the further course of the *CATeW* project.

The individual application of VC results in a maximum tripfuel reduction of roughly 1.5 %. However, the reader should keep in mind that in this case only two outboard flaps have been considered. Therefore, only limited beneficial influence on the lift distribution and thus on the induced drag component is possible. For the turbulent aircraft with two VC segments, this is demonstrated with the drag breakdown for an exemplary lift coefficient of $\mathrm{C_L} = 0.45$ in table 4.

Table 4 – Drag breakdown for $\mathrm{C_L} = 0.45$

Parameter	Unit	turb. Ref	turb. 2 VC segments	Δ, [%]
AoA	°	1.22	0.98	-19.67
$\mathrm{C_{D,ind}}$	dc	59.33	58.78	-0.93
$\mathrm{C_{D,visc}}$	dc	155.84	155.66	-0.12
$\mathrm{C_{D,wav}}$	dc	11.63	9.52	-18.14
$\mathrm{C_{D,total}}$	dc	226.8	223.96	-1.25

For the chosen lift coefficient, a flap setting of 0° for the left flap and 3° for the right flap, respectively, is used (cf. Fig. 19b). Figure 24 illustrates the effect on the lift distribution for this specific lift coefficient and flap setting.

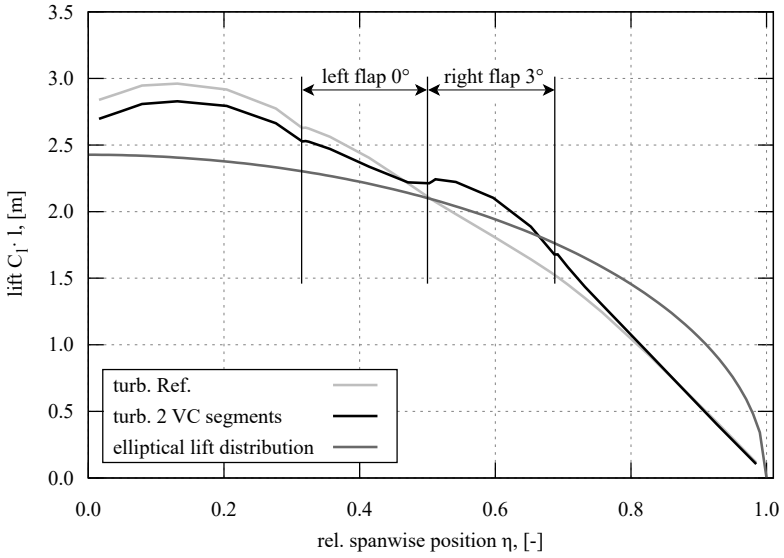

Figure 24 – Comparison of lift distributions for $\mathrm{C_L} = 0.45$

In addition to the distributions for both aircraft, an elliptical lift distribution is included since this one is considered most beneficial in terms of induced drag for a fixed wingspan [49]. Due to the flap deflection of 3°, the local lift is increased. To maintain the total lift coefficient, the angle of attack of the aircraft is therefore decreased (cf. table 4). This results in the inboard lift distribution approaching the elliptical distribution. In total, this leads in a slight reduction of the induced drag coefficient. However, the reduction in wave drag is more significant. The combination of those effects leads to the overall drag reduction. The value of the final tripfuel reduction is consistent with the results presented by Stephan et al. [36]. In this work, it was found, however, that an additional inboard ADHF flap and the associated possibility to influence the lift distribution result in a significant increase of the aero-

dynamic potential. For this inboard flap, negative deflection angles are found to be beneficial during cruise. Nonetheless, for the outboard flaps, deflections with $\delta > 2^\circ$ are not used during cruise [36]. The maximum deflection angle utilized in the work at hand is $\delta = 3^\circ$ indicating the existence of an upper boundary above which detrimental effects decrease aerodynamic performance.

The most relevant findings of this work can be summarized as follows:

- The final aircraft with combined application of HLFC and VC reveal significant potential on overall aircraft design level. The resulting reductions in required tripfuel are higher than the theoretical sum of the single technologies; this indicates the successful use of synergy effects of the two technologies.
- Different flap settings are used throughout the cruise flight making an aerodynamic database with various combinations of input parameters, such as lift coefficients and deployment angles, mandatory for this approach. This confirms the findings of the conducted pre-studies on airfoil level.
- The split outboard flap increases the overall performance only slightly; instead, the use of an additional inboard ADHF flap should be investigated in further research.
- For the use cases in this work, deflections with neither $\delta < 0^\circ$ nor $\delta > 3^\circ$ are beneficial in terms of $\mathrm{L/D}$ and are consequently not chosen during cruise flight. The lower boundary, however, may be shifted if an inboard flap is considered. Further analyses with different use cases should be conducted to narrow down uniform boundaries for the VC application in MICADO; these boundaries could then be incorporated in the database setup.

6 Conclusion

In this work, we presented a method to assess the combined application of hybrid laminar flow control and variable camber on overall aircraft design level. Since the method foresees the integration of an aerodynamic airfoil database in the preliminary aircraft design environment MICADO, initial studies were conducted on airfoil level first. Although the results indicate potential for efficient use of synergy effects between the two technologies, it became clear that it must be decided individually for the current freestream conditions whether or not an additional flap deflection is useful. After a detailed description of the new method, it was applied to several use cases. To map the individual influences of the single technologies, a stepwise approach was chosen starting with a turbulent medium range reference aircraft. As expected, both technologies show potential to improve the aerodynamics and thus the overall aircraft performance. The combination of both even increases the individual improvements resulting in a reduction of the tripfuel of almost 5 %. This was achieved using two outboard ADHF flaps.

To further improve the aerodynamic potential, various aspects for future research have been identified. It was already shown that the use of different airfoil geometries and suction areas can increase the HLFC potential significantly. However, an HLFC retrofit design is naturally limited in its maximum potential. To overcome this, new wing design methodologies are required using a possible laminarization as a driving design factor; such a method, which uses more aerodynamic airfoil information and an automatized airfoil selection process, is a current research topic at ILR. Considering the VC potential, the next step is to investigate the influence of an additional inboard ADHF flap. This flap adds more options to not only improve the off-design performance but also the lift distribution and thus the induced drag in the design point. However, the conscious tailoring of the lift distribution for the design point using the twist of the wing might reduce the potential of this additional flap. These two options and the associated detrimental effects on the aircraft, such as increased masses due to complex twist distributions, will be assessed against each other in follow-up studies.

7 Acknowledgements

The presented work has been carried out in the project *CATeW* (Coupled Aerodynamic Technologies for Aircraft Wings), funded by the German national research funding scheme LuFo VI-1 (Luftfahrtforschungsprogramm). The authors would like to acknowledge the support of the German Federal Ministry for Economic Affairs and Climate Action (BMWK).

8 Contact Author Email Address

The contact author email address is: tim.effing@ilr.rwth-aachen.de

9 Copyright Statement

References

[1] International Air Transport Association (IATA). *Aviation & Climate Change: Fact Sheet*. 2020.

[2] *Flightpath 2050: Europe's Vision for Aviation - Maintaining Global Leadership & Serving Society's Needs: Report of the High-Level Group on Aviation Research*. Policy / European Commission. Luxembourg: Publications Office of the European Union, 2011.

[3] International Air Transport Association (IATA). *Aircraft Technology Roadmap to 2050*. 2019.

[4] A. L. Braslow. *A History of Suction-Type Laminar-Flow Control with Emphasis on Flight Research*. Ed. by NASA History Division. 13th ed. Monographs in Aerospace History. Washington, D.C, 1999.

[5] R. D. Joslin. *Overview of Laminar Flow Control: Technical Report*. Ed. by National Aeronautics and Space Administration. 1998.

[6] G. Schrauf and H. von Geyr. "Simplified Hybrid Laminar Flow Control for the A320 Fin: Aerodynamic and System Design, First Results". In: *AIAA Scitech 2020 Forum*. Ed. by American Institute of Aeronautics and Astronautics. 2020.

[7] Boeing Commercial Airplane Company. *Assessment of Variable Camber for Application to Transport Aircraft*. Tech. rep. NASA-CR-158930. NASA Langley Research Center, Hampton, VA, 1980.

[8] J. Szodruch. "The Influence of Camber Variation on the aerodynamics of Civil Transport Aircraft". In: *AIAA 23st Aerospace Sciences Meeting*. Ed. by American Institute of Aeronautics and Astronautics. 1985.

[9] A. Bolokin and G. B. Gilyard. *Estimated Benefits of Variable-Geometry Wing Camber Control for Transport Aircraft*. Ed. by NASA Langley Research Center. 1999.

[10] P. Edi. "The Application of Hybrid Laminar Flow Control and Variable Camber Flap as a Flow Control on the Wing for Regional Aircraft Family". In: *23rd International Congress of Aeronautical Sciences*. Ed. by International Council of the Aeronautical Sciences. 2002.

[11] K. Risse, E. Anton, T. Lammering, K. Franz, and R. Hörnschemeyer. "An Integrated Environment for Preliminary Aircraft Design and Optimization". In: *53rd AIAA/ASME/ASCE/AHS/ASC Structures, Structural Dynamics and Materials Conference: SciTech 2012*. Ed. by American Institute of Aeronautics and Astronautics. Vol. AIAA 2012-1675. 2012.

[12] F. Schültke, B. Aigner, T. Effing, P. Strathoff, and E. Stumpf. "MICADO: Overview of Recent Developments within the Conceptual Aircraft Design and Optimization Environment". In: *69. Deutscher Luft- und Raumfahrtkongress*. Ed. by Deutsche Gesellschaft für Luft- und Raumfahrt - Lilienthal - Oberth e.V. 2020.

[13] F. Schültke and E. Stumpf. “UNICADO - Development and Establishment of a University Conceptual Aircraft Design Environment”. In: *69. Deutscher Luft- und Raumfahrtkongress*. Ed. by Deutsche Gesellschaft für Luft- und Raumfahrt - Lilienthal - Oberth e.V. 2020.

[14] G. Schrauf. “Status and perspectives of laminar flow”. In: *The Aeronautical Journal* 109.1102 (2005), pp. 639–644.

[15] H. Schlichting and K. Gersten. *Boundary-Layer Theory*. Springer Berlin, Heidelberg, 2017.

[16] H. L. Reed and W. S. Saric. “Stability of Three-Dimensional boundary layers”. In: *Annual Review of Fluid Mechanics* 21 (1989), pp. 235–284.

[17] K.-H. Horstmann, G. Schrauf, D. M. Sawyers, and H. Sturm. “A Simplified Suction System for an HLFC Leading Edge Box of an A320 Fin”. In: *CEAS Aerospace Aerodynamics Research Conference*. Ed. by Council of European Aerospace Societies. Vol. 91. 2002, pp. 1–7.

[18] G. Schrauf and H. von Geyr. “Hybrid Laminar Flow Control on A320 Fin: Retrofit Design and Sample Results”. In: *Journal of Aircraft* 58.6 (2021), pp. 1272–1280.

[19] F. Peter, K. Risse, F. Schültke, and E. Stumpf. “Variable Camber Impact on Aircraft Mission Planning”. In: *53rd AIAA Aerospace Sciences Meeting 2015*. Ed. by American Institute of Aeronautics and Astronautics. Vol. AIAA 2015-1902. Red Hook, NY: Curran, 2015.

[20] S. Barbarino, O. Bilgen, R. M. Ajaj, M. I. Friswell, and D. J. Inman. “A Review of Morphing Aircraft”. In: *Journal of Intelligent Material Systems and Structures* 22.9 (2011), pp. 823–877.

[21] P. Edi. “A Flow Control for an Advanced Technology Regional Aircraft (ATRA) Using a Variable Camber Wing with Hybrid Laminar Flow Control”. In: *3rd IASME/WSEAS Int. Conf. on FLUID DYNAMICS & AERODYNAMICS*. 2005, pp. 96–101.

[22] H. Hansen. “Laminar Flow Technology - The Airbus View”. In: *27th International Congress of the Aeronautical Sciences*. Ed. by International Council of the Aeronautical Sciences. 2010.

[23] P. Iannelli, J. Wild, M. Minervino, H. Strüber, F. Moens, and A. Vervliet. “Design of a High-Lift System for a Laminar Wing”. In: *5th European Conference for Aeronautics and Space Sciences*. Ed. by EUCASS Association. 2013.

[24] N. T. Nguyen et al. “Wind Tunnel Investigation of a Flexible Wing High-Lift Configuration with a Variable Camber Continuous Trailing Edge Flap Design”. In: *33rd AIAA Applied Aerodynamics Conference*. Ed. by American Institute of Aeronautics and Astronautics. Vol. AIAA 2015-2417. 2015.

[25] D. Reckzeh. “Der intelligente Tragflügel: Multifunktionale Klappen an der A350 XWB und der Weg zu zukünftigen Konzepten”. In: *Luft- und Raumfahrt* 1 (2018), pp. 22–25.

[26] N. Nguyen, K. Trinh, K. Reynolds, J. Kless, M. Aftosmis, and J. Urnes. “Elastically Shaped Wing Optimization and Aircraft Concept for Improved Cruise Efficiency”. In: *51st AIAA Aerospace Sciences Meeting including the New Horizons Forum and Aerospace Exposition*. Reston, VA: American Institute of Aeronautics and Astronautics, 2013.

[27] D. Reckzeh. “Multifunctional Wing Moveables: Design of the A350XWB and the Way to Future Concepts”. In: *29th Congress of the International Council of the Aeronautical Sciences* (2014).

[28] K. Risse. “Preliminary Overall Aircraft Design with Hybrid Laminar Flow Control”. Ph.D. thesis. RWTH Aachen University, 2016.

[29] M. Drela. *A User’s Guide to MSES 3.05*. Tech. rep. [user guide]. Cambridge, MA, 2007.

[30] G. Schrauf. *COCO: A Program to Compute Velocity and Temperature Profiles for Local and Nonlocal Stability Analysis of Compressible, Conical Boundary Layers with Suction*. Tech. rep. ZARM [user guide]. Bremen, Germany, 1998.

[31] G. Schrauf. *LILO 2.1: User’s Guide and Tutorial*. Tech. rep. GSSC 6 [user guide]. Bremen, Germany, 2006.

[32] J. Reneaux, J. Preist, J. C. Juillen, and D. Arnal. “Control of Attachment Line Contamination”. In: *2nd European Forum on Laminar Flow Technology*. 1996.

[33] M. Jentys, T. Effing, C. Breitsamter, and E. Stumpf. “Numerical Analyses of a Reference Wing for Combination of Hybrid Laminar Flow Control and Variable Camber”. In: *CEAS Aeronautical Journal, under Review* (2022).

[34] G. Schrauf. *Transition Criteria for HLFC Studies*. Tech. rep. PR1517186. Bremen, Germany, 2015.

[35] J. Anderson. *Fundamentals of Aerodynamics*. 6th ed. New York, NY: McGraw Hill Education, 2017.

[36] R. Stephan, N. Schneiders, F. Schültke, F. Peter, and E. Stumpf. “Evaluation of a Distributed Variable-Camber Trailing-Edge Flap System at Preliminary Aircraft Design Stage”. In: *AIAA AVIATION 2022 Forum*. Reston, VA: American Institute of Aeronautics and Astronautics, 2022.

[37] T. Pe and F. Thielecke. “Synthesis and Topology Study of HLFC System Architectures in Preliminary Aircraft Design”. In: *3rd CEAS Air & Space Conference*. Ed. by Council of European Aerospace Societies. 2011.

[38] F. Schültke and E. Stumpf. “Implementation of an Airfoil Information Database for Usage in Conceptual Aircraft Wing Design Process”. In: *AIAA Scitech 2019 Forum*. Ed. by American Institute of Aeronautics and Astronautics. Vol. 2019-0814. Reston, VA: American Institute of Aeronautics and Astronautics, 2019, p. 624.

[39] D. P. Raymer. *Aircraft Design: A Conceptional Approach: AIAA Education Series*. 6. AIAA education series. Washington, DC: American Institute of Aeronautics and Astronautics, 2018.

[40] W. H. Mason. “Analytic models for technology integration in aircraft design”. In: *Aircraft Design and Operations Meetings*. Ed. by American Institute of Aeronautics and Astronautics. 1990.

[41] C. W. Boppe. “Aircraft Drag Analysis Methods”. In: *Special Course on Engineering Methods in Aerodynamic Analysis and Design of Aircraft*. Ed. by North Atlantic Treaty Organization. Vol. AGARD-R-783. 1992, pp. 7.1–7.50.

[42] K.-H. Horstmann. “Ein Mehrfach-Traglinienverfahren und seine Verwendung für Entwurf und Nachrechnung nichtplanarer Flügelanordnungen”. Ph.D. thesis. Deutsche Forschungs- und Versuchsanstalt für Luft- und Raumfahrt, 1987.

[43] K.-H. Horstmann, T. Engelbrecht, and C. Liersch. *LIFTING_LINE: Version 3.0*. Tech. rep. [user guide]. 2019.

[44] F. Peter, E. Stumpf, M. Kintscher, I. Dimino, and A. Concilio. “Morphing Value Assessment on Overall Aircraft Level”. In: *Smart Intelligent Aircraft Structures (SARISTU)*. Ed. by P. C. Wölcken and M. Papadopoulos. Springer, Cham, 2016, pp. 859–871.

[45] T. Effing, F. Schültke, and E. Stumpf. “Investigation of the influence of the Reynolds number on the prediction accuracy of laminar drag components”. In: *67. Deutscher Luft- und Raumfahrtkongress*. Ed. by Deutsche Gesellschaft für Luft- und Raumfahrt - Lilienthal - Oberth e.V. 2018.

[46] S. Wöhler, J. Hartmann, E. Prenzel, and H. Kwik. “Preliminary aircraft design for a midrange reference aircraft taking advanced technologies into account as part of the AVACON project for an entry into service in 2028”. In: *67. Deutscher Luft- und Raumfahrtkongress*. Ed. by Deutsche Gesellschaft für Luft- und Raumfahrt - Lilienthal - Oberth e.V. 2018.

[47] T. Effing, F. Schültke, and E. Stumpf. “HLFC-optimized retrofit aircraft design of a medium-range reference configuration within the AVACON project”. In: *CEAS Aeronautical Journal* 12.2 (2021), pp. 441–456.

[48] T. Effing and E. Stumpf. *Laminarisierung der Tragflächen fortschrittlicher Flugzeugkonzepte: Final report for German LuFo V-3 project AVACON (RWTH Aachen University)*. Technische Informationsbibliothek Hannover, Germany, 2022.

[49] L. Prandtl. “Über Tragflügel kleinsten induzierten Widerstandes”. In: *Zeitschrift für Flugtechnik und Motorluftschiffahrt* 24 (1933), pp. 305–306.